

Echoes in a Single Quantum Kerr-nonlinear Oscillator

I. Tutunnikov,^{*} and K. V. Rajitha, and I. Sh. Averbukh
*AMOS and Department of Chemical and Biological Physics,
 The Weizmann Institute of Science, Rehovot 7610001, Israel*

Quantum Kerr-nonlinear oscillator is a paradigmatic model in cavity and circuit quantum electrodynamics, and quantum optomechanics. We theoretically study the echo phenomenon in a single impulsively excited (“kicked”) Kerr-nonlinear oscillator. We reveal two types of echoes, “quantum” and “classical” ones, emerging on the long and short time-scales, respectively. The mechanisms of the echoes are discussed, and their sensitivity to dissipation is considered. These echoes may be useful for studying decoherence processes in a number of systems related to quantum information processing.

I. INTRODUCTION

Echoes in physics can be defined as spontaneous delayed responses following a series of pulsed excitations. Perhaps the most famous example is the spin echo effect [1, 2] conceived by E. Hahn in 1950. The effect is induced by irradiating a collection of spins by two delayed magnetic field pulses, resulting in a magnetization response appearing at twice the delay between the pulses. Over the years, echoes have been discovered in various physical systems, such as systems consisting of many interacting/non-interacting particles, or single quantum particles. Examples of echoes in many-particle systems include photon echoes [3, 4], neutron spin echo [5], cyclotron echoes [6], plasma-wave echoes [7], cold atom echoes in optical traps [8–10], echoes in particle accelerators [11–14], echoes in free-electron lasers [15], and echoes in laser-kicked molecules [16–18]. In addition, echoes have been observed in single quantum systems, such as atoms interacting with a quantized mode of electromagnetic radiation [19, 20], and in single vibrationally excited molecules [21].

In this paper, we study echoes in a single impulsively excited quantum Kerr-nonlinear oscillator. In case of negligible damping and without external drive, the system is modeled by the Hamiltonian [22]

$$\hat{H}_0 = \hbar\omega\hat{a}^\dagger\hat{a} + \hbar\chi(\hat{a}^\dagger)^2\hat{a}^2, \quad (1)$$

where \hat{a}^\dagger and \hat{a} are the canonical creation and annihilation operators (satisfying the commutation relation $[\hat{a}, \hat{a}^\dagger] = 1$), ω is the fundamental frequency of the oscillator, and χ is the anharmonicity parameter. The echoes studied here do not require inhomogeneous broadening in an ensemble of many oscillators. On contrary, they occur in individual quantum systems, like in [19–21], and completely rely on their intrinsic unitary dynamics.

The exactly solvable model described by the Hamiltonian in Eq. (1) [23–25], and its driven damped extensions [22] have been extensively studied theoretically. For the recent theoretical developments in this direction, see [26]

and the references therein. In modern experiments, specially designed superconducting quantum circuits allow studying the dynamics of the dissipationless system [see Eq. (1)], including the phenomena of state collapse and quantum revivals [27]. Such circuits are important in the context of quantum computing, and are used in developing various state preparation [28] and state protection [29] protocols. For recent reviews of quantum computing applications see, e.g. the references in [28, 29]. The Hamiltonian in Eq. (1) also describes quantum nonlinear mechanical and opto-mechanical mesoscopic oscillatory systems [30, 31].

The paper is organized as follows. In Sec. II, we introduce the interaction term used to model the impulsive excitation, and define the corresponding classical Kerr-nonlinear oscillator model. In Sec. III, the classical and quantum echoes are presented, and the mechanisms of their formation are discussed. In Sec. IV, we consider the effects of dissipation. Finally, Sec. V concludes the paper.

II. THE MODEL

A. Quantum model

We begin by considering a quantized Kerr-nonlinear oscillator “kicked” by a pulsed coherent field. The system including the external field is modeled by the Hamiltonian $\hat{H} = \hat{H}_0 + \hat{H}_{\text{int}}$, where the interaction term is given by [22]

$$\hat{H}_{\text{int}} = E_0 f(t) (e^{-i\omega_L t} \hat{a}^\dagger + e^{i\omega_L t} \hat{a}). \quad (2)$$

Here, ω_L is the carrier frequency of the external field, E_0 is its peak amplitude, and $f(t)$ defines the time dependence of the amplitude. The interaction term \hat{H}_{int} is written under the rotating wave approximation, assuming $|\omega_L - \omega| \ll \omega$ [32].

For convenience, we apply the unitary transformation $|\psi\rangle = e^{-i\omega_L \hat{a}^\dagger \hat{a} t} |\psi_L\rangle$, which removes the oscillating factors, $\exp(\pm i\omega_L t)$ from the Hamiltonian. The details are summarized in Appendix A. After the unitary transfor-

^{*} Corresponding author: ilia.tutunnikov@weizmann.ac.il

mation, the Hamiltonian reads [22]

$$\hat{H}_L = \hbar\Delta\hat{a}^\dagger\hat{a} + \hbar\chi(\hat{a}^\dagger)^2\hat{a}^2 + E_0f(t)(\hat{a}^\dagger + \hat{a}), \quad (3)$$

where $\Delta = \omega - \omega_L$ is the detuning. To simplify the notation, the subindex L is omitted in the rest of the paper.

We introduce dimensionless parameters $\tilde{\Delta} = \Delta/\chi$, $\tilde{E}_0 = E_0/(\hbar\chi)$, and time $\tilde{t} = t\chi$, such that the Hamiltonian in Eq. (3) becomes

$$\hat{\mathcal{H}} = \tilde{\Delta}\hat{a}^\dagger\hat{a} + (\hat{a}^\dagger)^2\hat{a}^2 + \tilde{E}_0\tilde{f}(\tilde{t})(\hat{a}^\dagger + \hat{a}), \quad (4)$$

where energy is measured in units of $\hbar\chi$.

B. Corresponding classical model

A dimensionless classical Hamiltonian, formally corresponding to the quantum one in Eq. (4), can be defined in terms of the complex variable a and its complex conjugate a^* , $\mathcal{H} = \tilde{\Delta}a^*a + (a^*)^2a^2 + \tilde{E}_0\tilde{f}(\tilde{t})(a^* + a)$. For mechanical systems, the variable a is expressed in terms of dimensionless classical coordinate \tilde{q} and momentum \tilde{p} , $a = (\tilde{q} + i\tilde{p})/\sqrt{2}$, where $\tilde{q} = q/\sqrt{\hbar/\omega m}$, $\tilde{p} = p\sqrt{\hbar\omega m}$, m is the mass of the oscillator, and ω is the fundamental frequency of the oscillator. The appearance of \hbar in these definitions is purely to allow a convenient comparison with the quantum case [23]. In terms of \tilde{q} and \tilde{p} , the classical Hamiltonian reads

$$\mathcal{H} = \frac{\tilde{\Delta}}{2}(\tilde{q}^2 + \tilde{p}^2) + \frac{1}{4}(\tilde{q}^2 + \tilde{p}^2)^2 + \sqrt{2}\tilde{E}_0\tilde{f}(\tilde{t})\tilde{q}. \quad (5)$$

In the rest of this paper, we use the scalings defined in this section, and omit the tildes to simplify the notation.

III. ECHO EFFECT: NEGLIGIBLE DAMPING

In this section, we study echoes in an impulsively excited Kerr-nonlinear oscillator. We begin from considering the free evolution of an oscillator initially prepared in a coherent state. Then, we consider the case when a pulsed excitation is applied after a delay τ . The results of direct numerical simulation are qualitatively explained and compared with approximate analytical results.

A. Evolution of a free oscillator

Initially, the oscillator is in a coherent state $|\alpha_0\rangle$. In terms of number states $\{|n\rangle\}$ (defined by $\hat{a}^\dagger\hat{a}|n\rangle = n|n\rangle$) it is given by

$$|\psi(t=0)\rangle = |\alpha_0\rangle = e^{-|\alpha_0|^2/2} \sum_{n=0}^{\infty} \frac{\alpha_0^n}{\sqrt{n!}} |n\rangle, \quad (6)$$

where α_0 is a complex number defining the coherent state. The wave function of the oscillator at time t reads

$$|\psi(t)\rangle = e^{-|\alpha_0|^2/2} \sum_{n=0}^{\infty} \frac{\alpha_0^n}{\sqrt{n!}} e^{-iE_n t} |n\rangle, \quad (7)$$

where $E_n = (\Delta - 1)n + n^2$ is the energy of the state $|n\rangle$ [see Eq. (4), with $E_0 = 0$]. To follow the wave packet dynamics, we use the expectation value of the operator $\hat{q} = (\hat{a}^\dagger + \hat{a})/\sqrt{2}$, which represents position in the case of mechanical systems [33], or one of the field quadratures in the case of a quantized cavity mode [34, 35]. It can be shown (see Appendix B) that for the state in Eq. (7) the expectation value $\langle\hat{q}\rangle(t)$ is given by

$$\langle\hat{q}\rangle(t) = \frac{e^{-|\alpha_0|^2}}{\sqrt{2}} [\alpha_0 \exp(|\alpha_0|^2 e^{-2it} - i\Delta \cdot t) + \text{c.c.}], \quad (8)$$

where c.c. stands for “complex conjugate”. Figure 1 shows an example curve for $\langle\hat{q}\rangle(t)$ obtained using Eq. (8) with $\Delta = 0$, and $\alpha_0 = 4$. As can be seen from the figure [and from Eq. (8)], the signal is π periodic due to the quantum revivals [36–38] the wave packet experiences at $t = kT_{rev} = k\pi$, $k = 1, 2, \dots$

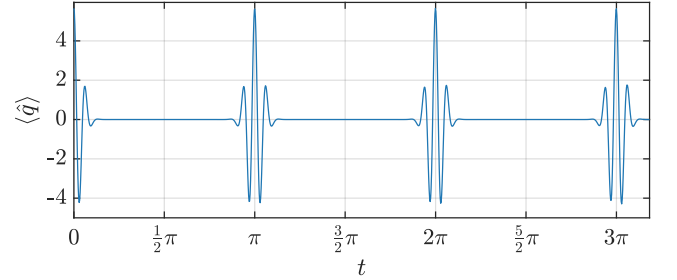


Figure 1. The function $\langle\hat{q}\rangle(t)$ [see Eq. (8)] with $\Delta = 0$ and $\alpha_0 = 4$.

Expanding the inner exponents, $\exp(\pm 2it)$ in Eq. (8) up to the second order results in an approximate expression describing the behavior of $\langle\hat{q}\rangle(t)$ in the vicinity of quantum revivals ($t \approx k\pi$, $k = 1, 2, \dots$)

$$\langle\hat{q}\rangle(t) \approx \alpha_0 e^{-2|\alpha_0|^2 t^2} \cos(2t|\alpha_0|^2 - \Delta \cdot t). \quad (9)$$

The function in Eq. (9) oscillates at frequency $2|\alpha_0|^2$ and decays to zero on a time-scale of $t_c = 1/(2|\alpha_0|)$, i.e. $\langle\hat{q}\rangle \propto \exp[-t^2/(2t_c^2)]$, which is the duration of the so-called “wave packet collapse”. The reason behind the collapse is the non-equidistant energy spectrum of the Kerr-nonlinear oscillator. In other words, the frequencies of the $|n\rangle$ states (forming the initial wave packet) are not integer multiples of the fundamental frequency ω , and, as a result, the states quickly step out of phase.

B. Evolution of an impulsively excited oscillator

Next, we consider results of an impulsive excitation (a “kick”) applied after a delay τ (counted from the beginning of the evolution) to the oscillator being initially

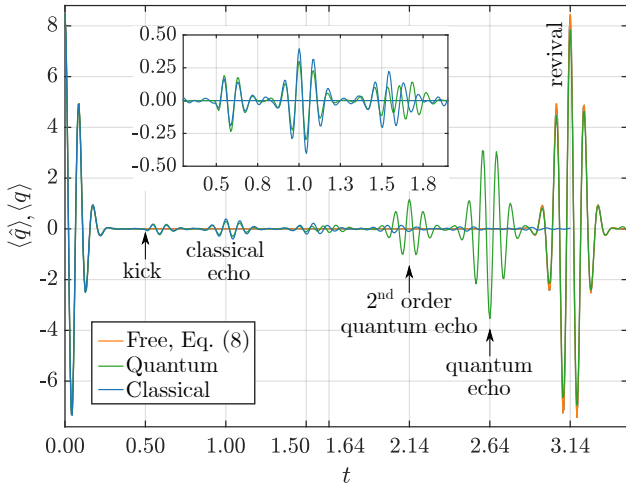


Figure 2. Quantum and classical echoes in kicked Kerr-nonlinear oscillator. $\langle \hat{q} \rangle(t)$ is the quantum expectation value, while $\langle q \rangle(t)$ is the average position of $N = 5 \times 10^4$ classical oscillators. The detuning parameter is $\Delta = 0.01$. The initial coherent state is defined by $\alpha_0 = 6$. The kick is applied at $t = \tau = 0.5$. An immediate response to the excitation can be seen. The classical echo emerges at $t = 2\tau = 1.0$. The quantum echo of the first order appears at $t = T_{rev} - \tau = 2.64$, while the second order quantum echo is centered at $t = T_{rev} - 2\tau = 2.14$ ($T_{rev} = \pi$). Excitation is Gaussian in time, $E_0 f(t) = E_0 \exp[-(t - \tau)^2/\sigma^2]$, with $E_0 = 3.0$ and $\sigma = 0.01$. The inset shows a magnified portion of the plot.

in a coherent state $|\alpha_0\rangle$. Figure 2 shows the expectation value $\langle \hat{q} \rangle(t) = \langle \hat{a}^\dagger + \hat{a} \rangle / \sqrt{2}$ calculated numerically in two different ways: (i) by solving the time-dependent Schrödinger equation with Hamiltonian in Eq. (4), and (ii) by simulating the behavior of a classical ensemble corresponding to $|\alpha_0\rangle$. The curve describing the free propagation [see Eq. (8)] is added for comparison.

The behavior of the classical ensemble is studied with the help of the Monte Carlo approach. Hamilton's equations of motion, derived from the classical Hamiltonian in Eq. (5), are solved numerically for an ensemble of $N \gg 1$ oscillators. The initial position q_0 and momentum p_0 of the oscillators are distributed according to

$$P(q_0, p_0) \propto \exp \left[-\frac{(q_0 - \sqrt{2}\alpha_0)^2}{2\sigma_q^2} - \frac{p_0^2}{2\sigma_p^2} \right], \quad (10)$$

where $\sigma_q = \sigma_p = 1/\sqrt{2}$. This initial classical distribution corresponds to a coherent state $|\alpha_0\rangle$. The classical observable $\langle q \rangle(t)$ is the average position of the oscillators.

As seen in Fig. 2, the quantum and classical results are in good agreement during the initial stages of evolution. The kick is applied at $t = \tau = 0.5$, and both quantum and classical simulations predict the expected immediate response to the applied excitation. Later on, at twice the kick delay ($t = 2\tau = 1.0$), coherent oscillations appear again without any additional kicks. On the long time scale, several additional pulsed responses having re-

markably large amplitudes emerge at $t = T_{rev} - \tau = 2.64$, and $t = T_{rev} - 2\tau = 2.14$ ($T_{rev} = \pi$).

The described pulsed responses are similar to echo signals known in many other physical systems. The characteristic property of echoes is their timing—echoes appear at multiples of the kick delay, i.e. $t = \pm l\tau \bmod(T_{rev})$, where $l = 1, 2, \dots$. Here, we refer to echoes at $t = +l\tau \bmod(T_{rev})$ as “classical echoes of order l ”, because they emerge in the quasi-classical limit (see Fig. 2, at $t = 2\tau = 1.0$) and the mechanism behind their formation is classical. In contrast, echoes at $t = -l\tau \bmod(T_{rev})$ are of purely quantum origin. They emerge due to the quantum revivals phenomenon, and we refer to them as “quantum echoes of order l ” (see Fig. 2, at $t = T_{rev} - \tau = 2.64$ and $t = T_{rev} - 2\tau = 2.14$). Quantum echoes having similar timing were studied theoretically in ensembles of anharmonically confined atoms [10], and observed experimentally in a gas of laser-kicked linear molecules [17, 18, 39]. Similar effects, but unrelated to the revivals phenomenon, were also studied in ensembles of nonlinear systems with equidistant spectrum [40, 41].

Before proceeding further, it is important to emphasize the conceptual difference between the echoes observed in inhomogeneous ensembles of many particles and echoes in single particle systems [19–21]. In the latter case, including the echo in a single mode of electromagnetic field described by Hamiltonian in Eq. (4), the effect does not require inhomogeneous broadening of the particle properties, but relies solely on the quantum nature of the dynamics.

C. Quantum echo - mechanism of formation

To reveal the mechanism of echo formation, we begin by considering the limit of weak impulsive excitations. In this limit, the temporal extent of $f(t)$ [the function defining the time dependence of the kick, see Eq. (4)] is much shorter than unity (in units of χ^{-1}).

In the impulsive approximation, during the kick, the Hamiltonian in Eq. (4) can be approximated by $\hat{\mathcal{H}} \approx E_0 f(t)(\hat{a}^\dagger + \hat{a})$. This allows to model the effect of the kick as $|\psi_+\rangle \approx \exp(\beta \hat{a}^\dagger - \beta^* \hat{a}) |\psi_-\rangle$, where $|\psi_\pm\rangle$ are the wave functions before/after the kick, and $\beta = i\lambda = -iE_0 \int_{-\infty}^{\infty} f(t) dt$. The action of the kick is equivalent to application of the displacement operator $\hat{D}(\beta) = \exp(\beta \hat{a}^\dagger - \beta^* \hat{a})$, which shifts coherent states, $\hat{D}(\beta) |\alpha\rangle = \exp[(\alpha^* \beta - \alpha \beta^*)/2] |\alpha + \beta\rangle$.

The kick is applied at $t = \tau$, and at that moment the state of the oscillator reads

$$|\psi_-\rangle = e^{-|\alpha_0|^2/2} \sum_{n=0}^{\infty} \frac{\alpha_0^n}{\sqrt{n!}} e^{-iE_n \tau} |n\rangle. \quad (11)$$

Using the completeness property of coherent states, we expand each number state $|n\rangle$ in terms of coherent states

$$|n\rangle = \frac{1}{\pi} \int_{\mathbb{C}} e^{-|\alpha|^2/2} \frac{(\alpha^*)^n}{\sqrt{n!}} |\alpha\rangle d^2\alpha. \quad (12)$$

Immediately after the kick, the state is given by

$$|\psi_+\rangle \approx D(\beta) |\psi_-\rangle = \frac{e^{-|\alpha_0|^2/2}}{\pi} \times \sum_{n=0}^{\infty} \frac{\alpha_0^n}{n!} e^{-iE_n\tau} \int_{\mathbb{C}} e^{-|\alpha|^2/2} (\alpha^*)^n \hat{D}(\beta) |\alpha\rangle d^2\alpha. \quad (13)$$

Next, we expand each coherent state $|\alpha + \beta\rangle$ in terms of number states $\{|m\rangle\}$, and substitute $\beta = i\lambda$

$$|\psi_+\rangle = e^{-|\alpha_0|^2/2} \sum_{m,n=0}^{\infty} \frac{\alpha_0^n}{n!} \frac{1}{\sqrt{m!}} e^{-iE_n\tau} |m\rangle \times \frac{1}{\pi} \int_{\mathbb{C}} e^{-|\alpha|^2} (\alpha^*)^n e^{i\alpha\lambda - \lambda^2} (\alpha + i\lambda)^m d^2\alpha. \quad (14)$$

Up to the first order in λ (i.e. assuming $|\lambda| = E_0 \int_{-\infty}^{\infty} f(t) dt \ll 1$) the complex integral in Eq. (14) becomes

$$\frac{1}{\pi} \int_{\mathbb{C}} e^{-|\alpha|^2} (\alpha^*)^n [\alpha^m + i\lambda m \alpha^{m-1} + i\lambda \alpha^{m+1}] d^2\alpha. \quad (15)$$

The three resulting integrals can be evaluated by substituting $\alpha = r e^{i\varphi}$, changing variables $t = r^2$, and using the definition of the Gamma function $\Gamma(n) = \int_0^{\infty} e^{-t} t^{n-1} dt = (n-1)!$.

The state at time T (counted from the moment of the kick), is given by

$$|\psi(T)\rangle = |\psi_f(T)\rangle + |\psi_{-1}(T)\rangle + |\psi_1(T)\rangle, \quad (16)$$

where

$$\begin{aligned} |\psi_f(T)\rangle &= A \sum_{n=0}^{\infty} \frac{\alpha_0^n}{\sqrt{n!}} e^{-iE_n(\tau+T)} |n\rangle, \\ |\psi_{-1}(T)\rangle &= A \frac{i\lambda}{\alpha_0} \sum_{n=0}^{\infty} \frac{n\alpha_0^n}{\sqrt{n!}} e^{-i(E_{n-1}\tau + E_n T)} |n\rangle, \\ |\psi_1(T)\rangle &= A i\lambda \alpha_0 \sum_{n=0}^{\infty} \frac{\alpha_0^n}{\sqrt{n!}} e^{-i(E_{n+1}\tau + E_n T)} |n\rangle, \end{aligned} \quad (17)$$

and $A = \exp(-|\alpha_0|^2/2)$. After the weak kick, the state of the oscillator is composed of three wave packets. The first one, $|\psi_f\rangle$ is identical to the freely evolving initial coherent state $|\alpha_0\rangle$ [see Eq. (7)]. Using the expression for energy $E_n = (\Delta - 1)n + n^2$, the newly created wave packets read

$$\begin{aligned} |\psi_{-1}(T)\rangle &\propto \sum_{n=0}^{\infty} \frac{n[\alpha_0 e^{2i\tau}]^n}{\sqrt{n!}} e^{-iE_n(\tau+T)} |n\rangle, \\ |\psi_1(T)\rangle &\propto \sum_{n=0}^{\infty} \frac{[\alpha_0 e^{-2i\tau}]^n}{\sqrt{n!}} e^{-iE_n(\tau+T)} |n\rangle. \end{aligned} \quad (18)$$

This shows that $|\psi_1\rangle$ has the form of a coherent state $|\alpha_0 \exp(-2i\tau)\rangle$ propagating freely for the time $\tau + T$.

We proceed with the analysis of the expectation value of the operator $\hat{q} = (\hat{a}^\dagger + \hat{a})/\sqrt{2}$. It can be shown (see

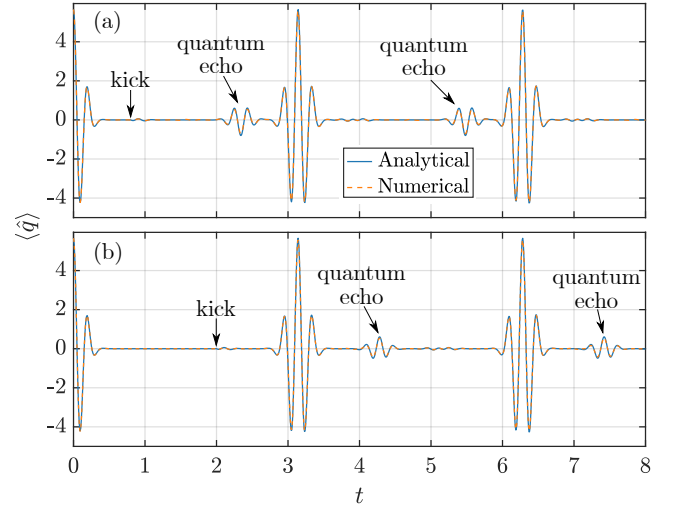


Figure 3. Comparison of the expectation value $\langle \hat{q} \rangle(t)$ obtained using Eq. (19) (solid blue), and numerically (dashed orange). Detuning parameter is $\Delta = 0.01$. The initial coherent state is defined by $\alpha_0 = 4$. The kick is applied at (a) $t = \tau = 0.8$, and (b) $t = \tau = 2.0$, while the first echo response emerges at $t = T_{rev} - \tau = 2.34$ and $t = 2T_{rev} - \tau = 4.28$, respectively. Excitation is Gaussian in time, $E_0 f(t) = E_0 \exp[-(t - \tau)^2/\sigma^2]$, with $E_0 = 0.50$, and $\sigma = 0.02$.

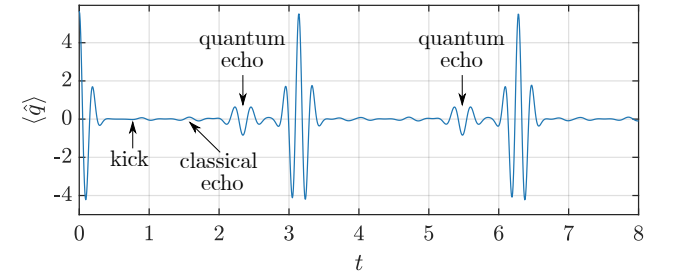


Figure 4. Numerically calculated quantum expectation value $\langle \hat{q} \rangle(t)$. The detuning parameter is $\Delta = 0.01$. The initial coherent state is defined by $\alpha_0 = 4$. The kick is applied at $t = \tau = 0.8$, and the immediate response to the excitation can be seen. Low-amplitude classical echo is visible at $t = 2\tau = 1.6$, while the quantum echo appears at $t = T_{rev} - \tau = 2.14$. Excitation is Gaussian in time, $E_0 f(t) = E_0 \exp[-(t - \tau)^2/\sigma^2]$, with $E_0 = 1.0$, and $\sigma = 0.1$.

Appendix C) that up to the terms first order in λ , $\langle \hat{q} \rangle(t)$ is given by

$$\begin{aligned} \langle \hat{q} \rangle(t) &= c_f(t) e^{z(t)} \\ &+ \lambda c_{-1}(t) e^{z(t-\tau)} + \lambda c_1(t) e^{z(t+\tau)} \\ &+ \text{c.c.}, \end{aligned} \quad (19)$$

where “c.c.” stands for complex conjugate, t is time counted from the beginning of the evolution, $z(t) = |\alpha_0|^2 e^{-2it}$, and $c_f(t) = \alpha_0 \exp(-|\alpha_0|^2 - i\Delta \cdot t)/\sqrt{2}$. The first term in Eq. (19) is identical to $\langle \hat{q} \rangle(t)$ of the freely evolving initial coherent state $|\alpha_0\rangle$ [see Eq. (8)], while the other two stem from the quantum interference of $|\psi_f\rangle$ and

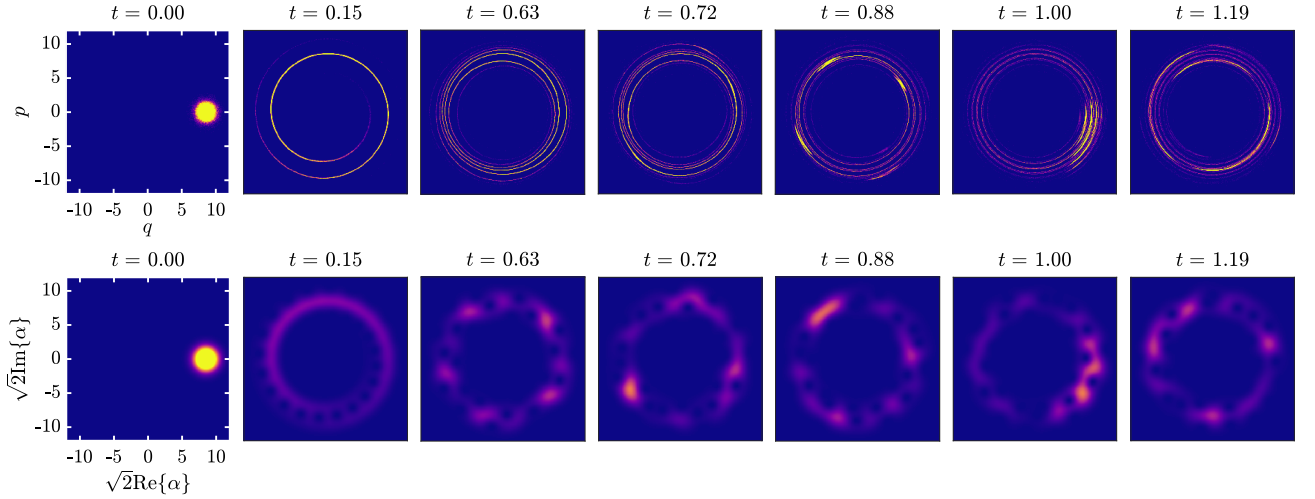


Figure 5. Top row - snapshots of the classical phase space distribution. Bottom row - corresponding Husimi Q-distribution. The detuning parameter is $\Delta = 0.01$. The initial coherent state is defined by $\alpha_0 = 6$. The kick is applied at $t = \tau = 0.50$. The snapshot at $t = 2\tau = 1.0$, shows how the bunches in the classical phase space distribution synchronize, producing the classical echo. Similar synchronization phenomenon is seen in the Q-distribution at the same moment. Excitation is Gaussian in time, $E_0 f(t) = E_0 \exp[-(t - \tau)^2/\sigma^2]$, with $E_0 = 15$, and $\sigma = 0.01$.

$|\psi_{\pm 1}\rangle$ [see Eq. (17)]. The time-dependent coefficients $c_{\pm 1}$ are defined in Appendix C [see Eq. (C20)]. The overall behavior of the two terms proportional to λ is determined by the functions $\exp[z(t \pm \tau)]$, which have a characteristic width of $t_c = 1/(2|\alpha_0|)$ [see Eqs. (8) and (9)].

The function $\exp[z(t - \tau)]$ is centered at $t = \tau$ (the moment of the kick) and describes the expected impulsive response to the kick, while $\exp[z(t + \tau)]$ is centered at $t = -\tau$. Both functions are π periodic, and therefore $\exp[z(t + \tau)]$ describes localized oscillations emerging periodically *before each revival*, at $t = kT_{rev} - \tau$, $k = 1, 2, \dots$. This delayed response is the previously discussed quantum echo of the first order (see Fig. 2 at $t = T_{rev} - \tau = 2.64$).

Figure 3 shows two examples in which the kick is applied at $\tau = 0.8$ [panel (a)], and $\tau = 2.0$ [panel (b)]. In Fig. 3(a), the quantum echo appears for the first time before the first revival, at $t = T_{rev} - \tau = \pi - \tau = 2.34$. In Fig. 3(b), the timing of the kick is such that the echo appears only before the second revival, at $t = 2T_{rev} - \tau = 2\pi - \tau = 4.28$. For the chosen kick parameters, the analytical result [see Eq. (19)] and the result of direct numerical solution of the time-dependent Schrödinger equation are in good agreement.

So far, we have demonstrated that the quantum echo at $t = T_{rev} - \tau$ is a first order effect in λ (the excitation strength parameter). In the next section, we show that the classical echo at $t = 2\tau$ [see Fig. (2)] emerges only in the second order of λ , which explains the dominating amplitude of the quantum echo.

As an additional numerical example, we consider the case of a kick having a slightly higher amplitude ($E_0 = 1.0$) and longer duration ($\sigma = 0.1$), which can not be treated within the impulsive approximation used to derive Eq. (19). Figure 4 shows that the first order quan-

tum echo still appears before the quantum revival, and also a weak classical echo is visible at $t = 2\tau$.

D. Classical echo - mechanism of formation

In this section, we consider the effects up to the second order in the kick strength λ , and discuss the emergence of the classical echo. It can be shown (see Appendix C) that up to the second order in λ , the expectation value of the operator $\hat{q} = (\hat{a}^\dagger + \hat{a})/\sqrt{2}$ is given by

$$\begin{aligned} \langle \hat{q} \rangle(t) &= [c_f(t) + \lambda^2 c_0(t)]e^{z(t)} \\ &+ \lambda \sum_{j=\pm 1} c_j(t)e^{z(t+j\tau)} \\ &+ \lambda^2 \sum_{j=\pm 2} c_j(t)e^{z(t+j\tau)} + \text{c.c.}, \end{aligned} \quad (20)$$

where “c.c.” stands for complex conjugate, $\lambda = -E_0 \int_{-\infty}^{\infty} f(t) dt$, $z(t) = |\alpha_0|^2 e^{-2it}$, and $c_f = \alpha_0 \exp(-|\alpha_0|^2 - i\Delta \cdot t)/\sqrt{2}$. The terms proportional to λ^2 introduce two new time points when the signal exhibits pulsed responses (echoes). The term $\exp[z(t + 2\tau)]$ corresponds to second order quantum echo appearing before each revival, at $t = kT_{rev} - 2\tau$, $k = 1, 2, \dots$. The term $\exp[z(t - 2\tau)]$ corresponds to a response appearing after an additional delay τ after the kick, at $t = 2\tau$. This is the classical echo of the first order. The time-dependent coefficients $c_{\pm 1, 2}$ are defined in Appendix C [see Eq. (C20)].

We can gain a physical insight into the mechanism of the classical echo formation by considering the classical phase space dynamics. Figure 5 shows a series of snapshots of the classical phase space distribution at several times before and after the kick applied at $t = \tau = 0.5$.

For comparison, the lower row shows the corresponding quantum Husimi Q-distribution, defined as [35]

$$Q(q, p, t) = Q(\sqrt{2}\text{Re}\{\alpha\}, \sqrt{2}\text{Im}\{\alpha\}, t) = \frac{1}{\pi} \langle \alpha | \hat{\rho} | \alpha \rangle,$$

where $\hat{\rho}$ is the density matrix of the oscillator (for a pure quantum state $\hat{\rho} = |\psi\rangle\langle\psi|$). In an anharmonic oscillator, the frequency (period) of oscillations is energy-dependent, or in other words, the period of oscillations depends on the radial distance from the phase space origin. As a result, with time, the initial smooth distribution at $t = 0$ evolves into a spiral-like structure (seen at $t = 0.15$). This filamentation of the phase space results in an increasing number of spiral turns, which become thinner in order to conserve the initial phase space volume (Liouville's theorem). Filamentation of the phase space is a known nonlinear phenomenon, which emerges in various physical systems, e.g. in the dynamics of stellar systems [42], and in accelerator physics [11, 13, 43].

The filamented phase space serves as a basis for the echo formation induced by a kick applied at the moment of well developed filamentation (at $t = \tau = 0.5$). The kick suddenly shifts the phase space distribution along the momentum axis, leading, with time, to the appearance of density bunches on the spiral. The panels corresponding to $t = 0.15, 0.63, 0.72$ show the creation of the bunches. As the time goes on, the bunches evolve into sharp “tips”. The tips are located on different turns of the spiral, therefore they rotate with different frequencies and step out of phase with time. However, at twice the kick delay (at $t = 2\tau = 1.0$) the bunches/tips synchronize. This synchronization is manifested as the classical echo effect [13, 17, 18, 44]. The similarity between the behavior of the classical phase space distribution and the Q-distribution is evident in Fig. 5. In principle, the synchronization recurs periodically with a period of τ . The so-called higher order classical echoes [13, 16, 17] (partially visible in Fig. 2 at $t = 3\tau = 1.5$) can be observed at higher multiples of the kick delay $t = 3\tau, 4\tau, \dots$

As a final remark for this section, we would like to point out the existence of the so-called “fractional echoes” in our system. These echoes are visible when higher moments of the field distribution are considered, e.g. $\langle \hat{q}^n \rangle$ $n \geq 2$ (see e.g. [17, 45, 46] and references therein). These echoes appear at rational fractions of the kick delay $k\tau/l$ (where k and l are mutually prime numbers) after the kick, and before/after revivals of various orders. Figure 6 shows the quantum expectation value of the operator $\hat{q}^2 = (\hat{a}^\dagger + \hat{a})^2/2$ demonstrating the regular and fraction quantum echoes at $t = T_{rev}/2 \pm \tau/2, T_{rev}/2 - \tau, T_{rev} \pm \tau/2, T_{rev} - \tau$, as well as low-amplitude classical fractional echo at $t \approx 3\tau/2$.

IV. ECHO EFFECT: DISSIPATION EFFECTS

In this section, we consider the role of damping effects caused by interaction of the oscillator with a reservoir

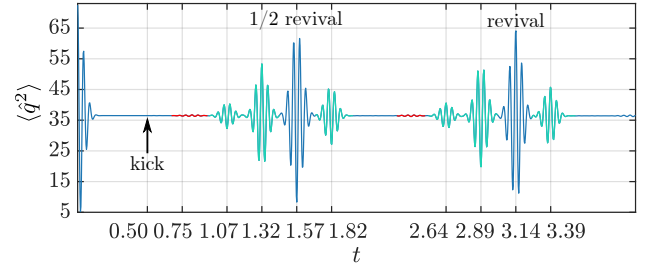


Figure 6. Fractional echoes in the expectation value $\langle \hat{q}^2 \rangle$. The kick is applied at $t = \tau = 0.5$. All the simulation parameters are identical to Fig. 2. Regular and fractional quantum echoes, marked in green, are visible at $t = T_{rev}/2 \pm \tau/2, T_{rev}/2 - \tau, T_{rev} \pm \tau/2, T_{rev} - \tau$. Low-amplitude classical echo, marked in red, is visible at $t \approx 3\tau/2$.

at finite temperature T . The whole system (oscillator + reservoir) is described by the time-dependent density matrix $\hat{\rho}(t)$. The oscillator is described by the reduced density matrix $\hat{S}(t) = \text{Tr}_R \hat{\rho}(t)$, where Tr_R denotes partial trace over the reservoir's degrees of freedom. We use the quantum optics model of a single mode of Kerr resonator interacting with a reservoir. In this model, $\hat{S}(t)$ satisfies the following differential equation [22, 47]

$$\begin{aligned} \frac{\partial \hat{S}}{\partial t} = & -i[\hat{\mathcal{H}}, \hat{S}] + \gamma \bar{n} [\hat{a}, \hat{S}], \hat{a}^\dagger \\ & + \frac{\gamma}{2} (2\hat{a}\hat{S}\hat{a}^\dagger - \hat{a}^\dagger\hat{a}\hat{S} - \hat{S}\hat{a}^\dagger\hat{a}), \end{aligned} \quad (21)$$

where $\hat{\mathcal{H}}$ is given in Eq. (4), $[\hat{A}, \hat{B}] = \hat{A}\hat{B} - \hat{B}\hat{A}$, γ is the dimensionless damping constant, $\bar{n} = [\exp(\epsilon) - 1]^{-1}$ [where $\epsilon = \hbar\omega/(k_B T)$] is the mean number of bosonic excitations in the reservoir's mode having frequency ω (the fundamental frequency of the quantized mode of the field), and k_B is the Boltzmann constant.

Figure 7 shows two examples of the damped dynamics of $\langle \hat{q} \rangle$ for the case of a field being initially in a coherent state $|\alpha_0\rangle$ [i.e. $\hat{S}(t=0) = |\alpha_0\rangle\langle\alpha_0|$]. For weak damping, $[\gamma = 10^{-3}$, see Fig. 7(a)], the amplitude of all oscillations (revivals and echoes) gradually diminish with each revival cycle. In the case of stronger damping, $[\gamma = 0.1$, see Fig. 7(b)], even the first revival at $t = T_{rev} = \pi$ is not visible. In contrast, the classical echo appearing on the short time scale is clearly visible. Since the quantum echo appears on the longer time scale (just before the revival), its amplitude is negligible as compared to the amplitude of the classical echo.

As an additional example, we consider the case of a field being initially in thermal equilibrium with the reservoir, i.e. the initial density matrix of the quantized mode is given by

$$\hat{S}(t=0) = \sum_{n=0}^{\infty} P_n |n\rangle\langle n| \quad P_n = \frac{1}{1 + \bar{n}} \left(\frac{\bar{n}}{1 + \bar{n}} \right)^n \quad (22)$$

where $\{P_n\}$ is the Bose-Einstein distribution. Figure 8 shows the damped dynamics of $\langle \hat{q} \rangle$, for both low and high

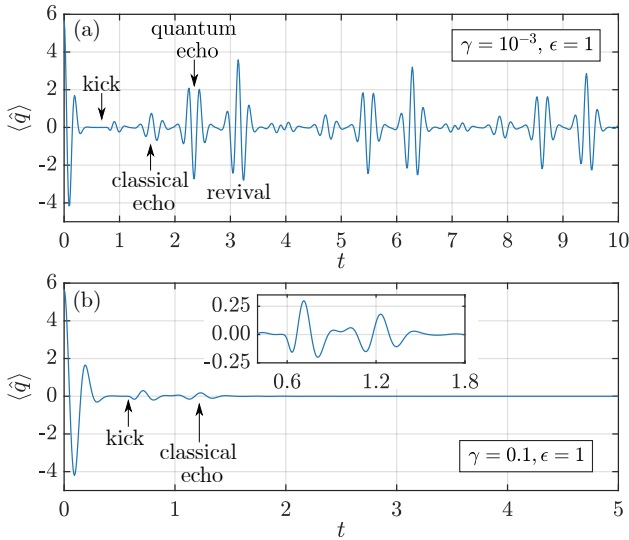


Figure 7. Numerically calculated quantum expectation value of the field quadrature operator $\hat{q} = (\hat{a}^\dagger + \hat{a})/\sqrt{2}$ for the case of initially coherent state defined by $\alpha_0 = 4$. The detuning parameter is $\Delta = 0.01$. (a) Weak damping ($\gamma = 10^{-3}$), the kick is applied at $t = \tau = 0.8$. (b) Strong damping ($\gamma = 0.1$), the kick is applied at $t = \tau = 0.6$. In both cases, the excitations are Gaussian in time, $E_0 f(t) = E_0 \exp[-(t - \tau)^2/\sigma^2]$, with $E_0 = 3.0$, and $\sigma = 0.02$.

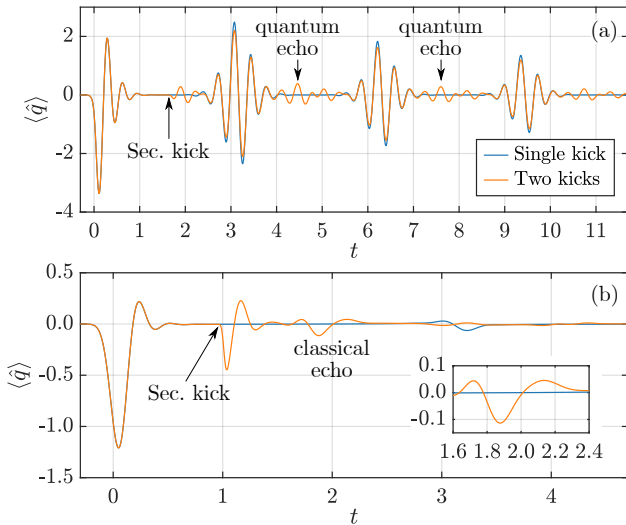


Figure 8. Numerically calculated quantum expectation value of the field quadrature operator $\hat{q} = (\hat{a}^\dagger + \hat{a})/\sqrt{2}$ for the case of initially thermal state and $\gamma = 5 \times 10^{-3}$. The detuning parameter is $\Delta = 0.01$. The excitations are Gaussian, and the time dependent amplitude is given by: $E_{01} \exp[-t^2/\sigma_1^2] + E_{02} \exp[-(t - \tau)^2/\sigma_2^2]$. (a) Low temperature $\epsilon = 1$, the second kick is applied at $t = \tau = 1.7$, with $E_{01} = 20$, $\sigma_1 = 0.1$ and $E_{02} = 1$, $\sigma_2 = 0.05$. (b) High temperature $\epsilon = 0.1$, the second kick is applied at $t = \tau = 1.0$, with $E_{01} = 20$, $\sigma_1 = 0.1$ and $E_{02} = 13$, $\sigma_2 = 0.02$.

temperature reservoirs, and $\gamma = 5 \times 10^{-3}$. Here, we apply two delayed kicks to the system. The first one is stronger and it initiates the dynamics, while the second delayed kick induces the echoes.

In the case of low temperature [see Fig. 8(a)], the first kick at $t = 0$ is followed by decaying oscillations of $\langle \hat{q} \rangle$ with each revival. The timing of the second kick is such that the first quantum echo appears at $t = 2T_{rev} - \tau$, similar to Fig. 3(b). For high temperature [see Fig. 8(b)], the oscillatory response to the first kick decays faster as compared to the previous case, due to wider distribution of initially populated states of the field. The second kick is applied after the response to the first kick has been decayed, and the classical echo arises at twice the kick delay, $t \approx 2\tau$. Since the contact with the hot reservoir leads to faster decoherence, even the first quantum revival is not visible in this case.

V. CONCLUSIONS

Two types of echoes, quantum and classical ones, are demonstrated in the kicked Kerr-nonlinear oscillator. The classical echoes exist on the short time-scale in the semi-classical limit, while the quantum ones show themselves near the quantum revivals of various order. For weak excitation, the amplitude of the quantum echoes is much higher than the classical ones. The reason is that the quantum echo emerges in the first order perturbation theory in the excitation strength, while the classical echo first appears in the second order.

The echoes discussed in the present paper are somehow different from echoes emerging in inhomogeneously broadened ensembles of many particles, e.g. spin echoes [1, 2]. Here, they take place in a single quantum object, and, in principle, can be observed in a single quantum oscillator. In this case, the measurement should be repeated many times starting from the same initial condition. The interference echo structure developing after many measurements is a time-domain analogue of spatial interference pattern appearing on a screen as a result of sending single electrons one-by-one through a double slit (the famous Feynman gedanken experiment, see [48] and references therein). Recently, a related phenomenon of echoes in single vibrationally excited molecules was observed [21].

The amplitudes of the various echoes are sensitive to the decoherence processes. In the presence of strong damping, the quantum echoes and revivals may be completely suppressed, because they emerge on the long time-scale. In contrast, classical echoes appear on the short time-scale and may still be measured. A similar situation was recently encountered in experiments [49–52] studying collisional rotational relaxation in dense molecular gases. Although the rotational revivals were essentially suppressed at high pressure, the classical alignment echoes were readily observable and successfully used to measure the relaxation rates.

ACKNOWLEDGMENTS

This work was partially supported by the Israel Science Foundation (Grant No. 746/15). I.A. acknowledges support as the Patricia Elman Bildner Professorial Chair. This research was made possible in part by the historic generosity of the Harold Perlman Family.

Appendix A: Unitary transformation [Eq. (3)]

The unitary transformation $|\psi\rangle = e^{-i\omega_L \hat{N}t} |\psi_L\rangle$, where $\hat{N} = \hat{a}^\dagger \hat{a}$, allows removing the oscillating factors, $\exp(\pm i\omega_L t)$ from the interaction term \hat{H}_{int} in Eq. (2). It can be shown that $|\psi_L\rangle$ satisfies the Shrödinger equation with the Hamiltonian

$$\hat{H}_L = \hbar\Delta\hat{a}^\dagger\hat{a} + \hbar\chi(\hat{a}^\dagger)^2\hat{a}^2 + e^{i\omega_L \hat{N}t}\hat{H}_{\text{int}}e^{-i\omega_L \hat{N}t}, \quad (\text{A1})$$

where $\Delta = \omega - \omega_L$ is the detuning. The time-dependent operators $\hat{a}_L^\dagger(t) = \exp(i\omega_L \hat{N}t)\hat{a}^\dagger\exp(-i\omega_L \hat{N}t)$ and $\hat{a}_L(t) = \exp(i\omega_L \hat{N}t)\hat{a}\exp(-i\omega_L \hat{N}t)$ appearing in Eq. (A1) satisfy the differential equations

$$\begin{aligned} \frac{\partial \hat{a}_L^\dagger(t)}{\partial t} &= i\omega_L e^{i\omega_L \hat{N}t} [\hat{N}, \hat{a}^\dagger] e^{-i\omega_L \hat{N}t}, \\ \frac{\partial \hat{a}_L(t)}{\partial t} &= i\omega_L e^{i\omega_L \hat{N}t} [\hat{N}, \hat{a}] e^{-i\omega_L \hat{N}t}, \end{aligned} \quad (\text{A2})$$

having solutions $\hat{a}_L^\dagger(t) = \hat{a}^\dagger \exp(i\omega_L t)$ and $\hat{a}_L(t) = \hat{a} \exp(-i\omega_L t)$. Substituting these into the Hamiltonian in Eq. (A1), results in

$$\hat{H}_L = \hbar\Delta\hat{a}^\dagger\hat{a} + \hbar\chi(\hat{a}^\dagger)^2\hat{a}^2 + E_0 f(t)(\hat{a}^\dagger + \hat{a}), \quad (\text{A3})$$

which is the Hamiltonian in Eq. (3).

Appendix B: Free propagation of a coherent state [Eq. (8)]

In this Appendix, we calculate the time-dependent quantum expectation value of the operator $\hat{q} = (\hat{a}^\dagger + \hat{a})/\sqrt{2}$ for the free oscillator being initially in a coherent state $|\alpha_0\rangle$ [see Eq. (6)]. The wave function at time t reads

$$|\psi(t)\rangle = e^{-|\alpha_0|^2/2} \sum_{n=0}^{\infty} \frac{\alpha_0^n}{\sqrt{n!}} e^{-iE_n t} |n\rangle, \quad (\text{B1})$$

where $E_n = (\Delta - 1)n + n^2$. Applying the operator \hat{a} to the wave function yields

$$\hat{a}|\psi(t)\rangle = e^{-|\alpha_0|^2/2} \sum_{n=1}^{\infty} \frac{\alpha_0^n}{\sqrt{n!}} e^{-iE_n t} \sqrt{n} |n-1\rangle. \quad (\text{B2})$$

For convenience, we change the index of summation n to $k = n - 1$, such that

$$\hat{a}|\psi(t)\rangle = e^{-|\alpha_0|^2/2} \sum_{k=0}^{\infty} \frac{\alpha_0^{k+1}}{\sqrt{k!}} e^{-iE_{k+1}t} |k\rangle. \quad (\text{B3})$$

The expectation value $\langle\psi(t)|\hat{a}|\psi(t)\rangle$ is given by

$$\begin{aligned} \alpha_0 e^{-|\alpha_0|^2 - i\Delta \cdot t} \sum_{n=0}^{\infty} \frac{(|\alpha_0|^2 e^{-2it})^n}{n!} |n\rangle = \\ \alpha_0 e^{-|\alpha_0|^2} \exp(|\alpha_0|^2 e^{-2it} - i\Delta \cdot t) \end{aligned} \quad (\text{B4})$$

where we used $E_{n+1} - E_n = \Delta + 2n$. The expectation value of $\langle\psi(t)|\hat{a}^\dagger|\psi(t)\rangle$ is the complex conjugate of Eq. (B4). Finally, we have

$$\begin{aligned} \langle\hat{q}\rangle &= \frac{1}{\sqrt{2}} \langle\hat{a}^\dagger + \hat{a}\rangle \\ &= \frac{e^{-|\alpha_0|^2}}{\sqrt{2}} [\alpha_0 \exp(|\alpha_0|^2 e^{-2it} - i\Delta \cdot t) + \text{c.c.}], \end{aligned} \quad (\text{B5})$$

where c.c. stands for “complex conjugate”.

Appendix C: Derivation of Eq. (20)

In this Appendix, we derive the formula for $\langle\hat{q}\rangle(t) = \langle\hat{a}^\dagger + \hat{a}\rangle/\sqrt{2}$ up to the second order in λ (the excitation strength parameter) for an oscillator being initially in a coherent state $|\alpha_0\rangle$, and which is impulsively kicked after a delay τ . We derive the expectation value $\langle\hat{a}\rangle$ only, because $\langle\hat{a}^\dagger\rangle = \langle\hat{a}\rangle^*$. At the moment of the kick ($t = \tau$), the wave function reads

$$|\psi_-\rangle = e^{-|\alpha_0|^2/2} \sum_{n=0}^{\infty} \frac{\alpha_0^n}{\sqrt{n!}} e^{-iE_n \tau} |n\rangle. \quad (\text{C1})$$

Using the completeness of coherent states, we expand each $|n\rangle$ state in terms of coherent states

$$|n\rangle = \frac{1}{\pi} \int_{\mathbb{C}} e^{-|\alpha|^2/2} \frac{(\alpha^*)^n}{\sqrt{n!}} |\alpha\rangle d^2\alpha. \quad (\text{C2})$$

In the impulsive approximation (for details see Subsection III C), the wave function immediately after the kick, reads

$$\begin{aligned} |\psi_+\rangle &\approx \hat{D}(\beta) |\psi_-\rangle = \frac{e^{-|\alpha_0|^2/2}}{\pi} \times \\ &\sum_{n=0}^{\infty} \frac{\alpha_0^n}{n!} e^{-iE_n \tau} \int_{\mathbb{C}} e^{-|\alpha|^2/2} (\alpha^*)^n \hat{D}(\beta) |\alpha\rangle d^2\alpha, \end{aligned} \quad (\text{C3})$$

where $\hat{D}(\beta) = \exp(\beta\hat{a}^\dagger - \beta^*\hat{a})$ is the displacement operator, which shifts coherent states $\hat{D}(\beta)|\alpha\rangle = \exp[(\alpha^*\beta - \alpha\beta^*)/2]|\alpha + \beta\rangle$. Then, we express each coherent state $|\alpha + \beta\rangle$ in terms of number states $\{|m\rangle\}$ and substitute

$\beta = i\lambda$, where $\lambda = -E_0 \int_{-\infty}^{\infty} f(t) dt$. After rearrangement, $|\psi_+\rangle$ reads

$$|\psi_+\rangle = e^{-|\alpha_0|^2/2} \sum_{m,n=0}^{\infty} \frac{\alpha_0^n}{n!} \frac{1}{\sqrt{m!}} e^{-iE_n\tau} |m\rangle \times \frac{1}{\pi} \int_{\mathbb{C}} e^{-|\alpha|^2} (\alpha^*)^n e^{i\alpha\lambda - \lambda^2} (\alpha + i\lambda)^m d^2\alpha. \quad (C4)$$

Keeping terms up to the second order in λ in the complex integral in Eq. (C4), results in

$$\frac{1}{\pi} \int_{\mathbb{C}} e^{-|\alpha|^2} (\alpha^*)^n [\alpha^m - \lambda^2(1+m)\alpha^m + i\lambda m\alpha^{m-1} + i\lambda\alpha^{m+1} + (\lambda^2/2)(m-m^2)\alpha^{m-2} - (\lambda^2/2)\alpha^{m+2}] d^2\alpha. \quad (C5)$$

The task now is to evaluate the six integrals in Eq. (C5)

$$I_f = \frac{1}{\pi} \int_{\mathbb{C}} e^{-|\alpha|^2} (\alpha^*)^n \alpha^m d^2\alpha, \quad (C6)$$

$$I_j = \frac{C_j(m)}{\pi} \int_{\mathbb{C}} e^{-|\alpha|^2} (\alpha^*)^n \alpha^{m+j} d^2\alpha,$$

where $j = -2, \dots, 2$, and the coefficients are defined as

$$C_{-2}(m) = (\lambda^2/2)(m-m^2), \quad C_2(m) = -(\lambda^2/2),$$

$$C_{-1}(m) = i\lambda m, \quad C_1(m) = i\lambda, \quad (C7)$$

$$C_0(m) = -\lambda^2(1+m).$$

To evaluate the integrals, we substitute $\alpha = re^{i\varphi}$, change variables $t = r^2$, and use the definition of the Gamma function, $\Gamma(n) = \int_0^{\infty} e^{-t} t^{2n} dt = (n-1)!$. This results in $I_f = n!$ and $I_j = C_j(m-j)!$. Substituting these back into Eq. (C4) and propagating each number state $|m\rangle$ by multiplying it with $\exp(-iE_m T)$, results in six sums

$$\Sigma_f = e^{-|\alpha_0|^2/2} \sum_{n=0}^{\infty} \frac{\alpha_0^n}{\sqrt{n!}} e^{-iE_n(\tau+T)} |n\rangle, \quad (C8)$$

$$\Sigma_j = e^{-|\alpha_0|^2/2} \sum_{n=0}^{\infty} \frac{C_j \alpha_0^{n+j}}{\sqrt{n!}} e^{-i(E_{n+j}\tau + E_n T)} |n\rangle.$$

Note: the time T here is counted from the moment of the application of the kick.

After acting with the operator \hat{a} , the first sum becomes

$$\hat{a}\Sigma_f = e^{-|\alpha_0|^2/2} \sum_{n=1}^{\infty} \frac{\alpha_0^n}{\sqrt{n!}} e^{-iE_n(\tau+T)} \sqrt{n} |n-1\rangle, \quad (C9)$$

and changing the index of summation from n to $k = n-1$, results in

$$\hat{a}\Sigma_f = e^{-|\alpha_0|^2/2} \sum_{k=0}^{\infty} \frac{\alpha_0^{k+1}}{\sqrt{k!}} e^{-iE_{k+1}(\tau+T)} |k\rangle. \quad (C10)$$

The rest of the sums become

$$\hat{a}\Sigma_j = e^{-|\alpha_0|^2/2} \sum_{n=1}^{\infty} \frac{C_j(n)\alpha_0^{n+j}}{\sqrt{(n-1)!}} \times e^{-i(E_{n+j}\tau + E_n T)} |n-1\rangle, \quad (C11)$$

and after changing the index of summation, the sums read

$$\hat{a}\Sigma_j = e^{-|\alpha_0|^2/2} \sum_{k=0}^{\infty} \frac{C_j(k+1)\alpha_0^{k+1+j}}{\sqrt{k!}} \times e^{-i(E_{k+1+j}\tau + E_{k+1} T)} |k\rangle. \quad (C12)$$

The expectation value $\langle \hat{a} \rangle$ involves the products $(\Sigma_f^* + \Sigma_{j_1}^*)(\hat{a}\Sigma_f + \hat{a}\Sigma_{j_2})$, where $j_{1,2} = -2, \dots, 2$. Without loss of generality, we assume α_0 is real, such that $\alpha^* = \alpha$ and $|\alpha|^2 = \alpha^2$. Considering the products second order in λ and expanding the exponentials using the expression for energy, the products read

$$\begin{aligned} \Sigma_f^* \hat{a}\Sigma_f &= \alpha_0 e^{-|\alpha_0|^2} \times \exp\{|\alpha_0|^2 e^{-2i(T+\tau)} - i\Delta \cdot (T+\tau)\}, \\ \Sigma_f^* \hat{a}\Sigma_j &= \alpha_0^{j+1} e^{-|\alpha_0|^2} \times \exp[-i(j+\Delta \cdot j + j^2)\tau - i\Delta \cdot (T+\tau)] \\ &\times \sum_{k=0}^{\infty} \frac{C_j(k+1) [\alpha_0^2 e^{-2i(T+\tau+j\tau)}]^k}{k!} \\ &j = -2, \dots, 2, \\ \Sigma_j^* \hat{a}\Sigma_f &= \alpha_0^{j+1} e^{-|\alpha_0|^2} \times \exp[-i(j-\Delta \cdot j - j^2)\tau - i\Delta \cdot (T+\tau)] \\ &\times \sum_{k=0}^{\infty} \frac{C_j^*(k) [\alpha_0^2 e^{-2i(T+\tau-j\tau)}]^k}{k!} \\ &j = -2, \dots, 2, \\ \Sigma_{j_1}^* \hat{a}\Sigma_{j_2} &= e^{-|\alpha_0|^2} \alpha_0^{j_1+j_2+1} \times \exp[-i\tau(j_1+j_2+j_2^2-j_1^2)] \\ &\times \exp\{-i\Delta \cdot [(j_2-j_1)\tau + (T+\tau)]\} \\ &\times \sum_{n=0}^{\infty} C_{j_1}^*(k) C_{j_2}(k+1) \frac{[\alpha_0^2 e^{-2i[T+\tau+(j_2-j_1)\tau]}]^k}{k!} \\ &j_{1,2} = \pm 1. \end{aligned} \quad (C13)$$

The first term $\Sigma_f^* \hat{a}\Sigma_f$ is independent of λ , and it identical to Eq. (B4), describing the free propagation of a coherent state. The rest of the terms are proportional to λ, λ^2 and arise due to the kick. The series in Eq. (C13) are of the form $\sum_{k=0}^{\infty} f(k) z^k / k!$, where $f(k)$ (the C_j s) are polynomials in k . Such series can be summed up, producing terms of the form $p(z)e^z$, where $p(z)$ is a polynomial in

z. The results are

$$\begin{aligned}
\Sigma_f^* \hat{a} \Sigma_j &= \alpha_0^{j+1} e^{-|\alpha_0|^2} \\
&\times \exp[-i(j + j\Delta + j^2)\tau - i\Delta \cdot (t + \tau)] \\
&\times g_j \left[\alpha_0^2 e^{-2i(T+\tau+j\tau)} \right] \exp \left[\alpha_0^2 e^{-2i(T+\tau+j\tau)} \right] \\
&j = -2, \dots, 2, \\
\Sigma_j^* \hat{a} \Sigma_f &= \alpha_0^{j+1} e^{-|\alpha_0|^2} \\
&\times \exp[-i(j - j \cdot \Delta - j^2)\tau - i\Delta \cdot (t + \tau)] \\
&\times h_j \left[\alpha_0^2 e^{-2i(T+\tau-j\tau)} \right] \exp \left[\alpha_0^2 e^{-2i(T+\tau-j\tau)} \right] \\
&j = -2, \dots, 2, \\
\Sigma_{j_1}^* \hat{a} \Sigma_{j_2} &= \alpha_0^{j_1+j_2+1} e^{-|\alpha_0|^2} e^{-i\Delta \cdot (T+\tau)} \\
&\exp\{-i[j_1 + j_2 + j_2^2 - j_1^2 + \Delta \cdot (j_2 - j_1)]\tau\} \\
&w_{j_1 j_2} \exp \left[\alpha_0^2 e^{-2i[T+\tau+(j_2-j_1)\tau]} \right] \\
&j_{1,2} = \pm 1,
\end{aligned} \tag{C14}$$

where the polynomials g_j , h_j , and w_{j_1, j_2} are given by

$$\begin{aligned}
g_{-2}(z) &= -\frac{\lambda^2}{2}(2z + z^2), & g_2(z) &= -\frac{\lambda^2}{2}, \\
g_{-1}(z) &= i\lambda(z + 1), & g_1(z) &= i\lambda, \\
g_0(z) &= -\lambda^2(z + 2),
\end{aligned} \tag{C15}$$

$$\begin{aligned}
h_{-2}(z) &= -\frac{\lambda^2}{2}z^2, & h_2(z) &= -\frac{\lambda^2}{2}, \\
h_{-1}(z) &= -i\lambda z, & h_1(z) &= -i\lambda, \\
h_0(z) &= -\lambda^2(z + 1),
\end{aligned} \tag{C16}$$

and

$$\begin{aligned}
w_{-1, -1}(z) &= \lambda^2(z^2 + 2z), & w_{-1, 1}(z) &= \lambda^2 z, \\
w_{1, -1}(z) &= \lambda^2(z + 1), & w_{1, 1}(z) &= \lambda^2.
\end{aligned} \tag{C17}$$

To simplify the notations, we define

$$\begin{aligned}
A_j &= \alpha_0^{j+1} e^{-|\alpha_0|^2} \\
&\times \exp\{-i[j(1 + \Delta) + j^2]\tau - i\Delta \cdot t\}, \\
B_j(t) &= \alpha_0^{j+1} e^{-|\alpha_0|^2} \\
&\times \exp\{-i[j(1 - \Delta) - j^2]\tau - i\Delta \cdot t\}, \\
C_{j_1, j_2}(t) &= \alpha_0^{j_1+j_2+1} e^{-|\alpha_0|^2} e^{-i\Delta \cdot t} \\
&\times \exp\{-i[j_1 + j_2 + j_2^2 - j_1^2 + \Delta \cdot (j_2 - j_1)]\tau\},
\end{aligned} \tag{C18}$$

where $z(t, j; \tau) = \alpha_0^2 e^{-2i(T+j\tau)}$, and t counts from the beginning of the evolution. Finally, the expectation value

of the operator $\hat{q} = (\hat{a}^\dagger + \hat{a})/\sqrt{2}$ reads

$$\begin{aligned}
\langle \hat{q} \rangle(t) &= [c_f + \lambda^2 c_0(t)] e^{z(t)} + \lambda \sum_{j=\pm 1} c_j(t) e^{z(t+j\tau)} \\
&+ \lambda^2 \sum_{j=\pm 2} c_j(t) e^{z(t+j\tau)} + \text{c.c.},
\end{aligned} \tag{C19}$$

where

$$\begin{aligned}
c_f &= \frac{A_0}{\sqrt{2}}, \\
\lambda^2 c_0(t) &= \frac{1}{\sqrt{2}} (A_0 g_0 + B_0 h_0 + \\
&+ C_{11} w_{11} + C_{-1, -1} w_{-1, -1}), \\
\lambda^2 c_{-2}(t) &= \frac{1}{\sqrt{2}} (A_{-2} g_{-2} + B_{-2} h_{-2} + C_{1, -1} w_{1, -1}), \\
\lambda^2 c_2(t) &= \frac{1}{\sqrt{2}} (A_2 g_2 + B_{-2} h_{-2} + C_{-1, 1} w_{-1, 1}), \\
\lambda c_{-1}(t) &= \frac{1}{\sqrt{2}} (A_{-1} g_{-1} + B_1 h_1), \\
\lambda c_1(t) &= \frac{1}{\sqrt{2}} (A_1 g_1 + B_{-1} h_{-1}).
\end{aligned} \tag{C20}$$

Figure 9 compares the expectation value $\langle \hat{q} \rangle(t)$ obtained using Eqs. (C19) and (C20), with the results of direct numerical integration of the time-dependent Shrödinger equation. The numerical result shows the overlapping classical echo of the second order and quantum echo of the third order between $t \approx 1.50$ and $t \approx 1.64$. These echoes are higher order effects that emerge in the third order perturbation theory in the parameter λ .

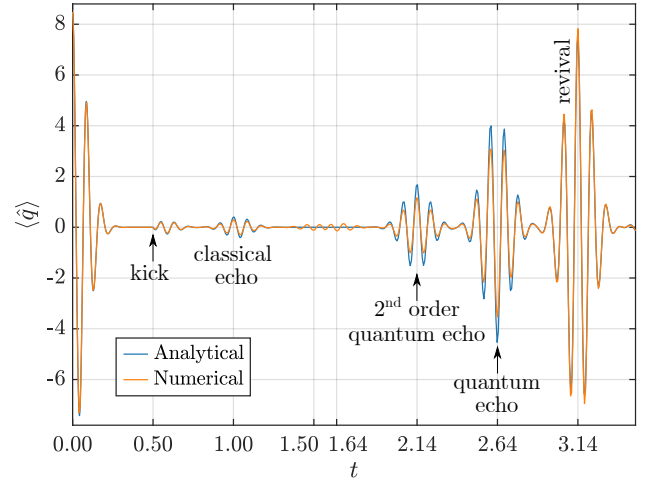


Figure 9. The quantum expectation value $\langle \hat{q} \rangle(t)$ obtained (i) using Eqs. (C19) and (C20), and (ii) numerically solving the time-dependent Shrödinger equation with the Hamiltonian in Eq. (4). The detuning parameter is $\Delta = 0.01$. Initial coherent state is defined by $\alpha_0 = 6$. The kick is applied at $t = \tau = 0.5$. Excitation is Gaussian in time, $E_0 f(t) = E_0 \exp[-(t - \tau)^2/\sigma^2]$, with $E_0 = 3.0$ and $\sigma = 0.01$. The parameters are identical to Fig. 2.

- [1] E. L. Hahn, “Spin Echoes,” *Phys. Rev.* **80**, 580 (1950).
- [2] E. L. Hahn, “Free nuclear induction,” *Phys. Today* **6**, 4 (1953).
- [3] N. A. Kurnit, I. D. Abella, and S. R. Hartmann, “Observation of a Photon Echo,” *Phys. Rev. Lett.* **13**, 567 (1964).
- [4] S. Mukamel, *Principles of nonlinear optical spectroscopy* (Oxford University Press, New York, 1995).
- [5] F. Mezei, “Neutron spin echo: A new concept in polarized thermal neutron techniques,” *Z. Physik* **255**, 146 (1972).
- [6] R. M. Hill and D. E. Kaplan, “Cyclotron Resonance Echo,” *Phys. Rev. Lett.* **14**, 1062 (1965).
- [7] R. W. Gould, T. M. O’Neil, and J. H. Malmberg, “Plasma Wave Echo,” *Phys. Rev. Lett.* **19**, 219 (1967).
- [8] A. Bulatov, A. Kuklov, B. E. Vugmeister, and H. Rabitz, “Echo in optical lattices: Stimulated revival of breathing oscillations,” *Phys. Rev. A* **57**, 3788 (1998).
- [9] F. B. J. Buchkremer, R. Dumke, H. Levens, G. Birkel, and W. Ertmer, “Wave Packet Echoes in the Motion of Trapped Atoms,” *Phys. Rev. Lett.* **85**, 3121 (2000).
- [10] M. Herrera, T. M. Antonsen, E. Ott, and S. Fishman, “Echoes and revival echoes in systems of anharmonically confined atoms,” *Phys. Rev. A* **86**, 023613 (2012).
- [11] G. Stupakov, “Echo effect in hadron colliders,” *Technical Report, SSCL-579* (1992), 10.2172/7237216.
- [12] L. K. Spentzouris, J.-F. Ostiguy, and P. L. Colestock, “Direct Measurement of Diffusion Rates in High Energy Synchrotrons Using Longitudinal Beam Echoes,” *Phys. Rev. Lett.* **76**, 620 (1996).
- [13] G. Stupakov, *Handbook of Accelerator Physics and Engineering*, 2nd ed., edited by A. W. Chau et. al (World Scientific, 2013) Chap. 2.3.13, pp. 121–123.
- [14] T. Sen and Y. S. Li, “Nonlinear theory of transverse beam echoes,” *Phys. Rev. Accel. Beams* **21**, 021002 (2018).
- [15] E. Hemsing, G. Stupakov, D. Xiang, and A. Zholents, “Beam by design: Laser manipulation of electrons in modern accelerators,” *Rev. Mod. Phys.* **86**, 897 (2014).
- [16] G. Karras, E. Hertz, F. Billard, B. Lavorel, J.-M. Hartmann, O. Faucher, E. Gershnabel, Y. Prior, and I. Sh. Averbukh, “Orientation and Alignment Echoes,” *Phys. Rev. Lett.* **114**, 153601 (2015).
- [17] K. Lin, P. Lu, J. Ma, X. Gong, Q. Song, Q. Ji, W. Zhang, H. Zeng, J. Wu, G. Karras, G. Siour, J.-M. Hartmann, O. Faucher, E. Gershnabel, Y. Prior, and I. Sh. Averbukh, “Echoes in Space and Time,” *Phys. Rev. X* **6**, 041056 (2016).
- [18] K. Lin, I. Tutunnikov, J. Ma, J. Qiang, L. Zhou, O. Faucher, Y. Prior, I. Sh. Averbukh, and J. Wu, “Spatiotemporal rotational dynamics of laser-driven molecules,” *Adv. Photon.* **2**, 1 (2020).
- [19] G. Morigi, E. Solano, B.-G. Englert, and H. Walther, “Measuring irreversible dynamics of a quantum harmonic oscillator,” *Phys. Rev. A* **65**, 040102 (2002).
- [20] T. Meunier, S. Gleyzes, P. Maioli, A. Auffeves, G. Nogues, M. Brune, J. M. Raimond, and S. Haroche, “Rabi Oscillations Revival Induced by Time Reversal: A Test of Mesoscopic Quantum Coherence,” *Phys. Rev. Lett.* **94**, 010401 (2005).
- [21] J. Qiang, I. Tutunnikov, P. Lu, K. Lin, W. Zhang, F. Sun, Y. Silberberg, Y. Prior, I. Sh. Averbukh, and J. Wu, “Echo in a single vibrationally excited molecule,” *Nat. Phys.* **16**, 328 (2020).
- [22] P. D. Drummond and D. F. Walls, “Quantum theory of optical bistability. I. Nonlinear polarisability model,” *J. Phys. A* **13**, 725 (1980).
- [23] G. J. Milburn, “Quantum and classical Liouville dynamics of the anharmonic oscillator,” *Phys. Rev. A* **33**, 674 (1986).
- [24] M. Stobińska, G. J. Milburn, and K. Wódkiewicz, “Wigner function evolution of quantum states in the presence of self-Kerr interaction,” *Phys. Rev. A* **78**, 013810 (2008).
- [25] M. Oliva and O. Steuernagel, “Quantum Kerr oscillators’ evolution in phase space: Wigner current, symmetries, shear suppression, and special states,” *Phys. Rev. A* **99**, 032104 (2019).
- [26] D. Roberts and A. A. Clerk, “Driven-Dissipative Quantum Kerr Resonators: New Exact Solutions, Photon Blockade and Quantum Bistability,” *Phys. Rev. X* **10**, 021022 (2020).
- [27] G. Kirchmair, B. Vlastakis, Z. Leghtas, S. E. Nigg, H. Paik, E. Ginossar, M. Mirrahimi, L. Frunzio, S. M. Girvin, and R. J. Schoelkopf, “Observation of quantum state collapse and revival due to the single-photon Kerr effect,” *Nature* **495**, 205 (2013).
- [28] S. Puri, S. Boutin, and A. Blais, “Engineering the quantum states of light in a Kerr-nonlinear resonator by two-photon driving,” *npj Quantum Inf.* **3**, 18 (2017).
- [29] N. Ofek, A. Petrenko, R. Heeres, P. Reinhold, Z. Leghtas, B. Vlastakis, Y. Liu, L. Frunzio, S. M. Girvin, L. Jiang, M. Mirrahimi, M. H. Devoret, and R. J. Schoelkopf, “Extending the lifetime of a quantum bit with error correction in superconducting circuits,” *Nature* **536**, 441 (2016).
- [30] M. Dykman, ed., *Fluctuating Nonlinear Oscillators: From Nanomechanics to Quantum Superconducting Circuits* (Oxford University Press, Oxford, 2012).
- [31] W. P. Bowen and G. J. Milburn, *Quantum Optomechanics*, 1st ed. (CRC Press, 2020).
- [32] P. Berman and V. S. Malinovsky, *Principles of laser spectroscopy and quantum optics* (Princeton University Press, Princeton, N.J., 2011).
- [33] C. Cohen-Tannoudji, B. Diu, and F. Laloë, *Quantum Mechanics, Volume 1: Basic Concepts, Tools, and Applications* (Wiley-VCH, 2020).
- [34] M. O. Scully and M. S. Zubairy, *Quantum Optics* (Cambridge University Press, 1997).
- [35] W. Schleich, *Quantum optics in phase space* (Wiley-VCH, Berlin New York, 2001).
- [36] J. Parker and C. R. Stroud, “Coherence and decay of Rydberg wave packets,” *Phys. Rev. Lett.* **56**, 716 (1986).
- [37] I. Sh. Averbukh and N. F. Perelman, “Fractional revivals: Universality in the long-term evolution of quantum wave packets beyond the correspondence principle dynamics,” *Phys. Lett. A* **139**, 449 (1989).
- [38] R. Robinett, “Quantum wave packet revivals,” *Phys. Rep* **392**, 1 (2004).
- [39] K. Lin, J. Ma, X. Gong, Q. Song, Q. Ji, W. Zhang, H. Li, P. Lu, H. Li, H. Zeng, J. Wu, J.-M. Hartmann, O. Faucher, E. Gershnabel, Y. Prior, and I. Sh. Averbukh, “Rotated echoes of molecular alignment: fractional, high order and imaginary,” *Opt. Express* **25**, 24917 (2017).

- [40] B. Y. Dubetskii and V. P. Chebotaev, “*Echoes in classical and quantum ensembles with determinate frequencies*,” *Pis'ma Zh. Eksp. Teor. Fiz.* **41**, 267 [JETP Lett. **41**, 328 (1985)] (1985).
- [41] B. Y. Dubetskii and V. P. Chebotaev, “*Imaginary echo in a gas in a Doppler expanded transition*,” *Izv. Akad. Nauk SSSR, Ser. Fiz.* **50**, 1530 [Bull. Acad. Sci. USSR, Phys. Ser. (English Transl.) **50**, 70 (1986)] (1986).
- [42] D. Lynden-Bell, “*Statistical Mechanics of Violent Relaxation in Stellar Systems*,” *Mon. Not. R. Astron. Soc.* **136**, 101 (1967).
- [43] G. Guignard, in *Frontiers of Particle Beams*, edited by M. Month and S. Turner (Springer Berlin Heidelberg, Berlin, Heidelberg, 1988) pp. 1–50.
- [44] G. V. Stupakov and S. K. Kauffmann, in *Proc. Par. Accel. Conf.*, Vol. 1 (1993) pp. 197–199.
- [45] G. Karras, E. Hertz, F. Billard, B. Lavorel, G. Siour, J.-M. Hartmann, O. Faucher, E. Gershnabel, Y. Prior, and I. Sh. Averbukh, “*Experimental observation of fractional echoes*,” *Phys. Rev. A* **94**, 033404 (2016).
- [46] B. Wang, L. He, Y. He, Y. Zhang, R. Shao, P. Lan, and P. Lu, “*All-optical measurement of high-order fractional molecular echoes by high-order harmonic generation*,” *Opt. Express* **27**, 30172 (2019).
- [47] W. Louisell, *Quantum statistical properties of radiation* (Wiley, New York, 1973).
- [48] R. Bach, D. Pope, S.-H. Liou, and H. Batelaan, “*Controlled double-slit electron diffraction*,” *New J. Phys* **15**, 033018 (2013).
- [49] D. Rosenberg, R. Damari, and S. Fleischer, “*Echo Spectroscopy in Multilevel Quantum-Mechanical Rotors*,” *Phys. Rev. Lett.* **121**, 234101 (2018).
- [50] H. Zhang, B. Lavorel, F. Billard, J.-M. Hartmann, E. Hertz, O. Faucher, J. Ma, J. Wu, E. Gershnabel, Y. Prior, and I. Sh. Averbukh, “*Rotational Echoes as a Tool for Investigating Ultrafast Collisional Dynamics of Molecules*,” *Phys. Rev. Lett.* **122**, 193401 (2019).
- [51] J. Ma, H. Zhang, B. Lavorel, F. Billard, E. Hertz, J. Wu, C. Boulet, J.-M. Hartmann, and O. Faucher, “*Observing collisions beyond the secular approximation limit*,” *Nat. Commun.* **10**, 5780 (2019).
- [52] J.-M. Hartmann, J. Ma, T. Delahaye, F. Billard, E. Hertz, J. Wu, B. Lavorel, C. Boulet, and O. Faucher, “*Molecular alignment echoes probing collision-induced rotational-speed changes*,” *Phys. Rev. Research* **2**, 023247 (2020).